PCCP

Cite this: *Phys. Chem. Chem. Phys.*, 2011, **13**, 17505–17510

www.rsc.org/pccp

PAPER

On the mechanism of enhanced oxygen reduction reaction in nitrogen-doped graphene nanoribbons†

Heejin Kim,[a] Kirak Lee,[b] Seong Ihl Woo[ab] and Yousung Jung*[a]

Received 24th May 2011, Accepted 31st August 2011
DOI: 10.1039/c1cp21665a

Nitrogen (N)-doped carbon materials were shown in recent studies to have promising catalytic activity for oxygen reduction reaction (ORR) as a metal-free alternative to platinum, but the underlying molecular mechanism or even the active sites for high catalytic efficiency are still missing or controversial both experimentally and theoretically. We report here the results of periodic density functional theory (DFT) calculations about the ORR at the edge of a graphene nanoribbon (GNR). The edge structure and doped-N near the edge are shown to enhance the oxygen adsorption, the first electron transfer, and also the selectivity toward the four-electron, rather than the two-electron, reduction pathway. We find that the outermost graphitic nitrogen site in particular gives the most desirable characteristics for improved ORR activity, and hence the active site. However, the latter graphitic nitrogen becomes pyridinic-like in the next electron and proton transfer reaction *via* the ring-opening of a cyclic C–N bond. This inter-conversion between the graphitic and pyridinic sites within a catalytic cycle may reconcile the controversy whether the pyridinic, graphitic, or both nitrogens are active sites.

1. Introduction

In a proton exchange membrane fuel cell (PEMFC), the rate of the cathode reaction, namely oxygen reduction reaction (ORR), is much slower than the rate of the anode reaction,[1,2] and many studies have been focused on improving the ORR activities using various catalysts. Generally, platinum based materials are known as the most efficient catalysts for ORR,[3] but platinum is a precious metal, has a limited amount of deposits on earth, and is hence very expensive to be commercialized.[4] Recently, the carbon-based materials with large surface area such as carbon nanotubes (CNT), nanofibers, and graphene have received attention as alternative metal-free catalyst materials to platinum.[5–14] In particular, nitrogen (N)-doped carbon materials have been experimentally shown to yield high ORR activity in the manner of the four-electron pathway.[5,11,14] Matter *et al.*[10,11] reported that the N-doped carbon nanofibers have high ORR catalytic activity, and the N-doped CNTs[6] and graphene[8,12] were also recently reported to have high activity for ORR even in the absence of transition metal atoms. But it is still controversial experimentally which compositions and structures are the active sites for ORR due to an indirect nature of experimental techniques to identify active sites.[13] The pyridinic-N sites (nitrogen atoms with lone pair electrons) have been widely received as catalytic active sites for ORR due to the delocalization of the π-electron from pyridinic-N,[15] and XPS experiments phenomenologically showed that the highly catalytic carbon materials usually have a large amount of pyridinic nitrogen.[7,8,10,13,14] On the contrary, a recent experiment using the same techniques suggested that the graphitic-N (nitrogen bonded to three sp^2 carbon atoms) was observed as the key for ORR activity rather than pyridinic-N.[16]

Theoretical studies have also been performed to understand the high ORR activity in N-doped carbon-based materials. Kurak and Anderson[17] showed that the doped nitrogen with ON–NH edge structure can catalyze the ORR in a two-electron pathway forming hydrogen peroxide. Okamoto[18] proposed that the four-electron ORR pathway can be achieved with an adequate binding energy of the oxygen atom on the multiple N-doped graphene center. Ikeda *et al.*[19] calculated the oxygen adsorption barriers and the subsequent ORR processes using Car–Parrinello molecular dynamics (CPMD)[20] simulations from which the graphitic-N site was proposed to be the catalytic active site. Recently, Shan and Cho[21] studied the N-doped CNTs and suggested that the Stone–Wales defect near the doped-N is a possible oxygen adsorption site for ORR due to the metallic electrons near the Fermi level.

As can be seen in this very brief summary of the literature on the subject, the question of active sites and the underlying mechanism for improved ORR activity are still controversial and unclear both experimentally and theoretically compared

[a] *Graduate school of EEWS (WCU), Korea Advanced Institute of Science & Technology (KAIST), Daejeon, Korea. E-mail: ysjn@kaist.ac.kr*
[b] *Department of Chemical and Biomolecular Engineering, KAIST, Daejoen, Korea*
† Electronic supplementary information (ESI) available. See DOI: 10.1039/c1cp21665a

to the platinum based materials.[22] In fact, because N should be placed on the edge or at the defect sites of the graphene to become a pyridinic-N, it is, despite some experimental attempts,[23] generally difficult to distinguish the effects of edge *vs.* pyridinic-N on the catalytic behavior to ORR.

In this work, we use density functional theory (DFT) calculations to identify the effect of edge, doped-N, and termination species on the ORR by using various graphene nanoribbon models. To this end, we suggest an ORR mechanism on the N-doped graphene nanoribbon and active sites that can reconcile different interpretations of XPS measurements for the active sites.

2. Computational methods

We performed the spin-polarized DFT calculations using the Vienna *Ab initio* Simulation Package (VASP)[24] with the Perdew–Burke–Ernzerhof (PBE) exchange-correlation functional[25] and the projector-augmented wave (PAW) method.[26] A plane wave basis with an energy cutoff of 400 eV was used and a $1 \times 4 \times 1$ Monkhorst–Pack *k*-points[27] mesh was sampled for the total energy calculation to give well converged energy values. A finer $1 \times 16 \times 1$ *k*-points mesh was used for the calculation of density of states (DOS). We considered a periodic nanoribbon with 56 carbon atoms as a model for N-doped graphene edges with hydrogen termination (Fig. 1), where the atomic positions were fully relaxed. It was reported in a recent experiment that the N-doping decreases surface oxygen-containing groups,[28] suggesting that the hydrogen terminated edge can be a reasonable model structure for N-doped graphene. More realistic graphene models surely would include various edge structures including termination species, defects, and geometric distortions. However the single graphene layer without these additional effects used in this work would enable us to focus on and pinpoint the effects of doped nitrogens and edges themselves without potential complications. The periodic box is represented with a dashed line in Fig. 1 and vacuum layers were set around 14 Å in the *x*- and *z*-direction to avoid interaction between slabs. Regardless of the existence of dopants and adsorbates, or the termination state of edge sites, the energy of the anti-ferromagnetic ordering was always lower than that of non-magnetic or ferromagnetic ordering by 0.02–0.28 eV, consistent with a previous report.[29] Therefore we performed all energy calculations in an anti-ferromagnetic ordering. To calculate the energy barriers associated with oxygen adsorption, we used the nudged elastic band (NEB) method[30] with eight images along the reaction path, also using spin-polarized formalism. The temperature and solvent effects are not considered explicitly in our calculations.

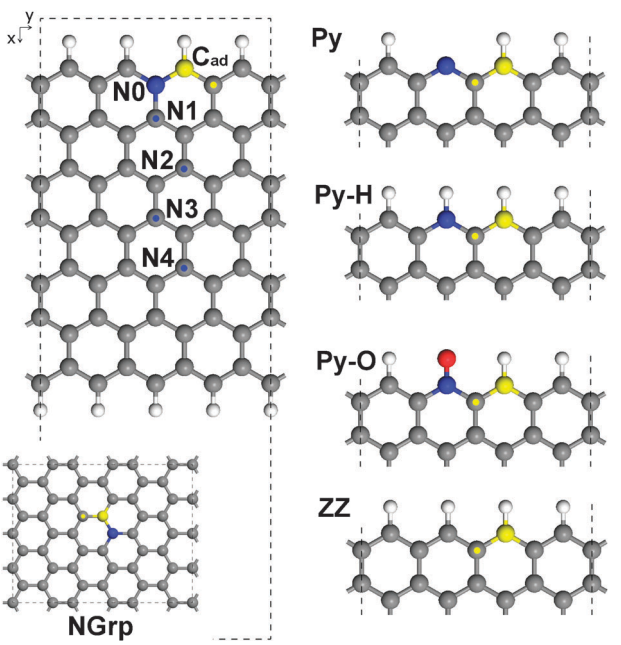

Fig. 1 The model structures with various geometries, N-doping sites, and edge states. The oxygen molecule is adsorbed at C_{ad} (yellow atom). The nitrogen, oxygen and hydrogen atoms are colored blue, red, and white, respectively, and the dotted line denotes a periodic boundary.

3. Results and discussions

3.1 Oxygen adsorption and the first electron transfer

There are two typical adsorption modes for an oxygen molecule, the side-on mode (also known as the Yeager model) and the end-on mode (known as the Pauling model).[31] We performed adsorption barrier calculations for both modes and the results are summarized in Table 1. Fig. 1 shows the model structures used in our calculations with different geometries, N-doping sites, and termination species. The oxygen molecule was considered to be adsorbed at the C_{ad} site (yellow atom), the edge carbon closest to the doped nitrogen for the end-on mode. Additional adsorption sites for the side-on mode are marked as small yellow dots in Fig. 1. For each graphitic type model (N1–N4) and pyridinic type model (Py, Py–H, Py–O), oxygen adsorption at the carbon site next to the doped-N was also examined but they either did not bind or gave higher adsorption barriers than the edge carbon site C_{ad}, and therefore are not considered further.

Table 1 The adsorption barriers of the oxygen molecule on the bulk graphene and graphene nanoribbons. Both side-on and end-on adsorption modes were calculated with the model structures shown in Fig. 1. The ΔO2p is the energy difference between the Fermi-level and the unoccupied 2p orbital state in the adsorbed oxygen molecule. Smaller ΔO2p means easier electron transfer to the oxygen to form superoxide

	Adsorption barrier/eV		
Model (Fig. 1)	Side-on	End-on	ΔO2p/eV
Grp	2.80	×[a]	1.930
NGrp	1.64	×[a]	1.660
ZZ	1.15	0.12	0.103
N0	—	0.35	0.010
N1	0.79	0.31	0.046
N2	0.93	0.21	0.069
N3	0.93	0.13	0.077
N4	1.01	0.12	0.100
Py	0.99	0.12	0.161
Py–H	1.05	0.85	0.033
Py–O	1.04	0.25	0.166

[a] × indicates that the adsorption of O_2 was unfavorable.

The oxygen molecule was adsorbed only as a side-on mode for the pristine (Grp) and N-doped (NGrp) models of the bulk graphene (center of the graphene). Adsorption barriers are 2.80 eV and 1.64 eV, respectively, and the energy states of adsorbed products are higher than those of the reactants (graphene + triplet O_2) by 2.14 eV and 1.36 eV, respectively. These results are consistent with earlier calculations on CNTs,[21,32] which indicates that the ORR is difficult to occur at the bulk graphene centers.

In contrast, oxygen adsorptions at the edge sites have considerably lower barriers, especially for the end-on mode. Regardless of the N-doping sites or the edge termination states, the adsorption of the end-on type is preferred for all zigzag edge structures both kinetically and energetically. Although Gong *et al.* suggested that N-doping may change the mode of oxygen adsorption from the end-on to side-on for CNTs,[6] it does not seem to be applicable for the GNR system or at the edge of graphene. Moreover, the speculation[6] that the induced positive charge of the carbon atom near the doped-N may facilitate the adsorption of an oxygen molecule is not supported by our calculations on the GNR edges. Instead, our calculations show that as the doped-N moves away from the oxygen adsorption site to more inner sites (from N0 to N4), the adsorption barrier decreases and converges to that of the pristine zigzag edge that has the lowest barrier. This may be explained by the fact that both nitrogen and oxygen are more electronegative than carbon, and thus they competitively withdraw electrons from carbon atoms and become partially negatively charged and repel each other. The hydrogen terminated structure (Py–H) has a relatively higher adsorption barrier than other structures.

In the overall ORR process under acidic conditions, the first electron transfer to the adsorbed oxygen molecule to form superoxide is usually considered as a rate determining step in carbon-based materials.[9,33,34] Tominaga *et al.*[35] evaluated the transferability of the first electron to oxygen by the energy difference (ΔO2p) between the Fermi level and the peak position of the density of states (DOS) in the unoccupied O-2p orbital for the adsorbed oxygen molecule. We performed the same analysis for our model structures with the results summarized in Table 1. The smaller ΔO2p means easier electron transfer to the oxygen molecule. The bulk graphene models (Grp and NGrp) show broad peaks for the unoccupied O-2p orbital around 2 eV above the Fermi level, meaning that the first electron transfer is difficult to occur. Along with the high oxygen adsorption barriers for the side-on mode described above, the reconfirmation by the orbital analysis, allowed us to conclude that the ordinary graphene centers cannot be the active sites toward ORR.

Contrarily, many edge structures show generally much smaller ΔO2p values facilitating easier first electron transfer, while Py (pyridinic-nitrogen) and Py–O have relatively larger ΔO2p compared to other edge sites, implying less activity. Due to a substantial adsorption barrier, the Py–H structure is also not likely to be an active site alone in the GNR system although it was previously suggested as an active site by Tominaga *et al.*[35] due to a relatively small ΔO2p value. It is noted that, although the doped-N did not lower the oxygen adsorption barriers at the ribbon edges (and rather increased them) as described in the previous paragraph, the existence of nitrogen reduces the ΔO2p and does help easier transfer of the first electron to the oxygen, a step regarded as rate determining.[9,33,34] In this point of view, the N0 structure with the smallest ΔO2p as well as a small adsorption barrier can be suggested as a most probable or better active site toward the ORR than other structures.

This then poses a question why the pyridinic-N, a generally accepted active site in many experimental interpretations, is less active than the N0 structure. Our calculations seem to be inconsistent with many experiments where highly active carbon materials usually have high contents of pyridinic nitrogen.[7,8,10,13,14] Thus, we investigated further the rest of the ORR steps using electrochemical approaches used by Kurak and Anderson[17] and Okamoto.[18] These two methods are essentially identical in the sense that the reversible potentials can be calculated using the thermodynamic data for reactions and binding energy difference between reactants and products. The detailed thermodynamic cycles used to calculate the reversible potentials are described in the ESI.†

3.2 Reversible potentials for ORR steps

The following ORR mechanism has been proposed for metal-free N-doped graphene surfaces ((1)-(2)-(3a)-(4)-(5))[18,19] and for glassy carbon ((1)-(2)-(3b)).[36,37]

$$\mathrm{Gr(aq) + O_2(g) \rightleftharpoons Gr{:}O_2{}^{ad}\,(aq)} \quad (1)$$

$$\mathrm{Gr{:}O_2{}^{ad}\,(aq) + H^+(aq) + e^- \rightleftharpoons Gr{:}OOH^{ad}(aq)} \quad (2)$$

$$\mathrm{Gr{:}OOH^{ad}(aq) + e^- \rightleftharpoons Gr{:}O^{ad}(aq) + OH^-(aq)} \quad (3a)$$

$$\mathrm{Gr{:}OOH^{ad}(aq) + e^- \rightleftharpoons Gr(aq) + OOH^-(aq)} \quad (3b)$$

$$\mathrm{Gr{:}O^{ad}(aq) + H^+(aq) + e^- \rightleftharpoons Gr{:}OH^{ad}(aq)} \quad (4)$$

$$\mathrm{Gr{:}OH^{ad}(aq) + H^+(aq) + e^- \rightleftharpoons Gr(aq) + H_2O(l)} \quad (5)$$

In eqn (1), the $Gr{:}O_2{}^{ad}$ (aq) denotes an oxygen molecule adsorbed on graphene in aqueous media. In step (2), the neutral OOH^{ad} species is formed by adding an electron and a proton to the adsorbed oxygen. The OOH^{ad} species then has two possible pathways to take in accepting an electron in step (3), one path by breaking the O–O bond to release OH^- and the other path by breaking the Grp–O bond to release OOH^-. The former corresponds to the four-electron reduction pathway that utilizes O^{ad}, and the latter corresponds to the two-electron reduction pathway to form an undesired product, H_2O_2. In step (4), the OH^{ad} species is formed, and in step (5), water is released and the catalytic graphene is regenerated. Okamoto[18] suggested that, in reaction (3a), the O–O bond breaking to form OH^- with the addition of electron and the formation of a water molecule by taking a proton occur stepwise, whereas in reaction (5), the proton and electron transfer occurs simultaneously to produce a water molecule. Other possible reaction pathways including the formation of hydrogen peroxide or the dissociative adsorption of the oxygen molecule on N-doped graphene were also considered systematically by Okamoto[18] but yielded reactions (1)–(5) to be the most plausible pathway for the four-electron reduction. Ikeda *et al.* also reported the same reaction pathway for the zigzag edge of graphene.[19]

Table 2 The calculated reversible potentials for each reduction step. The third and fourth columns are two different reduction reactions for OOH^{ad}

Model (Fig. 1)	(2) $O_2^{ad} \rightarrow OOH^{ad}$/V	(3) $OOH^{ad} \rightarrow$ (3a) $O^{ad} + OH^-$	(3) $OOH^{ad} \rightarrow$ (3b) OOH^-	(4) $O^{ad} \rightarrow OH^{ad}$/V	(5) $OH^{ad} \rightarrow H_2O$/V	Offset potential from $\Delta O2p^a$/V
ZZ	1.19	0.65	0.19	1.94	0.88	0.62
N0	1.00	2.02	0.42	0.73	0.96	0.87
N1	1.10	1.20	0.43	1.37	1.14	0.77
N2	1.10	1.06	0.39	1.52	1.09	0.71
N3	1.15	0.89	0.16	1.68	0.87	0.69
N4	1.15	0.81	0.17	1.77	0.86	0.63
Py	1.20	0.59	0.17	1.98	0.87	0.46
Py–H	1.14	1.80	0.99	0.76	1.71	0.81
Py–O	1.12	0.65	0.45	1.99	1.10	0.44

[a] The offset potentials are estimated by interpolating the calculated ΔO2p values here to those estimated by Tominaga *et al.*[35]

Following these proposed reaction steps, the reversible potentials were calculated from experimental thermodynamic data (ESI†). The results are summarized in Table 2. For comparison, the offset potentials estimated by interpolating the calculated ΔO2p values here to those estimated by Tominaga *et al.*[35] using the same calculation method are presented in the last column. Table 2 clearly shows that the offset potentials are mostly determined by the first electron transfer, *i.e.*, ΔO2p = 0.44–0.77 V *versus* the standard hydrogen electrode (SHE), as expected, since that step is generally believed to be rate limiting. For the N0 and Py–H structures, the ORR offset potentials are determined by the reduction reaction (4), 0.73 V and 0.76 V, respectively. Above the latter reversible potentials, the adsorbed oxygen atom will remain as a poisoning adsorbate blocking the active sites. Thus, the offset potentials are around 0.7 V for graphitic nitrogens (N0–N3), 0.6 V for a pristine zigzag GNR edge (ZZ), and 0.45 V for the pyridinic-N (Py) and the Py–O structure. As mentioned in the previous section, the ORR on the Py–H site would be limited by the oxygen adsorption step due to a high activation barrier.

Reaction (3a) or (3b), reduction of OOH^{ad}, is particularly notable since it determines whether the catalysis follows the four-electron or the two-electron reduction pathway. The reversible potentials indicate only the energy difference between the reactant and the product with an assumption of low activation barriers. Therefore, the selectivity for the (3a) over the (3b) path should be deduced based on both the binding energies and bond lengths of O–O and C–O in the OOH^{ad} species (Table 3) and the associated reversible potentials (Table 2). The N0 structure has the longest relative O–O bond length (~0.02 Å larger than the other structures) and shortest relative C–O bond lengths (~0.04 Å smaller than the other structures), implying the ease of breaking the O–O bond (four-electron pathway) in the N0 structure geometrically compared to other sites. Energetically also, the N0 is the only structure where the O–O bond is weaker than the C–O bond (by 0.31 eV), implying that the O–O bond cleavage is easier than the C–O. For all other structures, the C–O bond is weaker.

From a viewpoint of reversible potentials (Table 2), all edge structures seem to prefer the path (3a) to (3b), but the N0 structure has a particularly larger reversible potential toward the O–O bond breaking. On the basis of these results (Table 2 and 3), we can consider that the N0 structure has a higher selectivity toward the four-electron reduction reaction than the other edge structures. Again, the pyridinic nitrogen structure does not seem to be a direct source of improved ORR activity, where its characteristics are interestingly rather similar to those of the pristine zigzag edge (ZZ) structure in terms of adsorption barrier, ΔO2p, reversible potentials, and bond lengths.

Table 3 Bond strength of the O–O (BE_{O-O}) and C–O bonds (BE_{C-O}) in the OOH^{ad} species, with ΔBE being the difference between the two. A more positive ΔBE and longer d_{O-O} bond length can be an indicator for a higher selectivity toward the four-electron reduction

Model (Fig. 1)	BE_{O-O}/eV	BE_{C-O}/eV	ΔBE/eV	d_{O-O}/Å	d_{C-O}/Å
ZZ	−2.16	−1.34	−0.83	1.469	1.467
N0	−0.79	−1.10	0.31	1.488	1.432
N1	−1.61	−1.10	−0.51	1.467	1.469
N2	−1.75	−1.14	−0.62	1.472	1.466
N3	−1.92	−1.36	−0.55	1.470	1.464
N4	−2.00	−1.36	−0.64	1.470	1.464
Py	−2.22	−1.36	−0.86	1.476	1.450
Py–H	−1.01	−0.53	−0.47	1.469	1.471
Py–O	−2.16	−1.07	−1.09	1.492	1.447

Fig. 2a shows a partial density of state (PDOS) of the 2p-orbital for the nitrogen atom in the Py–N model. The small peaks around the Fermi-level are the $2p_z$ component and the larger peaks at −2 eV are the localized $2p_x$ component. In the orbital picture for the energy band located around −2 eV (Fig. 2b), somewhat localized electrons are seen at the edge of the nitrogen atom along the *x*-direction. These localized pictures along the plane direction are not observed in the other nitrogen models. Therefore these unpaired electrons in

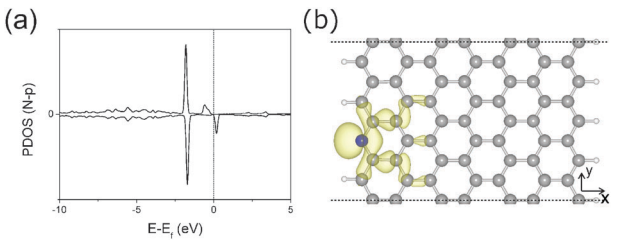

Fig. 2 (a) The partial density of state (PDOS) for the p-orbital of the pyridinic nitrogen atom in the Py structure. (b) The isosurface of electron density for the band with a peak position around −2 eV in (a). The nitrogen lone pair electrons are somewhat localized at the edge of the nitrogen atom (blue) along the *x*-direction.

the pyridinic nitrogen that are somewhat localized are perhaps reminiscent of the localized terminal C–H bond of the pristine zigzag edge, making the electronic states and properties of Py–N similar to those of the pristine zigzag edge with low ORR activity as shown in Table 1. A question then arises, why the highly active carbon materials have been phenomenologically observed to have a large amount of pyridinic nitrogens in many experiments.

3.3 On the active site for ORR

Based on the results described in the previous sections, namely, the easiest first electron transfer and the highest selectivity toward the four-electron reduction in the N0 structure, we propose that the N0 structure is the main catalytic active site. A schematic of the ORR cycle around the N0 structure is summarized in Fig. 3.

A notable feature is the state (III) with the OOH^{ad} species. In this state, due to a relative strength of the C–O *vs*. the O–O bond (Table 3), OOH^{ad} is easily dissociated into O^{ad} and OH^-. The remaining oxygen atom O^{ad} (becoming a carbonyl group) then cleaves the C–N bond in step (3a) to form a stable CHO group and the broken-bonded nitrogen atom then becomes pyridinic-N in (IV). This ring-opening of the graphene edge is not observed in the other model structures considered here. The PDOS and the orbital shape of the nitrogen in stage (IV), Fig. 4, are indeed similar to those of a typical pyridinic nitrogen in Fig. 2. The latter C–N bond-broken edge structure is also energetically more stable than the reference state ($N0 + 1/2O_2$) by around 0.8 eV, thus suggesting that it may be formed even in as-prepared N-doped carbon materials without any electrochemical cycling. If the graphene contains much oxygen before/after nitrogen doping or the synthesis is performed under oxidation conditions, the bond-broken pyridinic nitrogen structures such as (IV) can be preferably developed. We expect that this kind of pyridinic nitrogen atoms resulting from the ring-opening of the C–N graphene edge bonds may

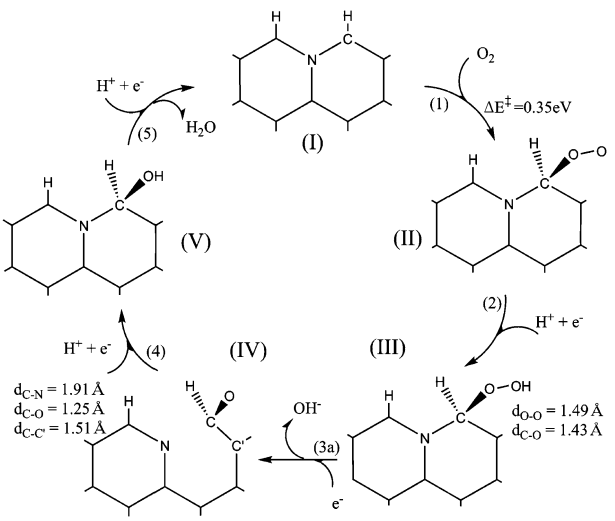

Fig. 3 The proposed ORR catalytic cycle for the N0 structure, showing only the catalytically active part of the GNR edge in Fig. 1. Arabic numerals next to the arrows in parentheses denote the reaction steps described in the text.

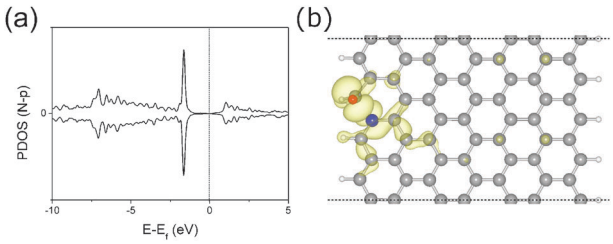

Fig. 4 (a) The partial density of state (PDOS) for the p-orbital of the nitrogen atom in the N0 structure in stage (IV) of Fig. 3. (b) The isosurface of electron density for the band of peak position around −2 eV. The blue and red atoms are nitrogen and oxygen, respectively.

be measured as highly active pyridinic-N sites in XPS measurements. Depending on the synthesis conditions, of course, it can also be measured as graphitic-N if it is in stage (I). When a hydrogen atom is attached to the oxygen O^{ad} in step (4), the broken C–N bond zips back and the nitrogen becomes again a graphitic-N in stage (V).

4. Conclusions

(1) Density functional calculations suggest that the reactive nature of edge structures by itself introduces possibilities of ORR activity in carbon materials by lowering the oxygen adsorption barrier and the first electron transfer barrier significantly.

(2) The nitrogen doping increases further the activity of graphene edges by enhancing the first electron transfer rate and the preference for the four-electron (rather than the two-electron) reduction pathway, the two most important steps for improved ORR performance responsible for the rate and selectivity.

(3) The N0 outermost graphitic nitrogen site among others yields the lowest barrier for the rate-limiting[9,32,33] first electron transfer as well as the highest selectivity toward the four-electron reduction pathway, and hence is proposed to be the main active site.

(4) The proposed catalytic cycle around the graphitic N0 site involves a ring-opening of the cyclic C–N bond at the edge of graphene which results in the pyridinic nitrogen.

(5) This new type of N-doped active site that inter-converts between pyridinic and graphitic-types may reconcile the experimental controversy whether the pyridinic, graphitic, or both types of nitrogen are the ORR active sites for N-doped graphene materials. We expect that not only the CHO functional groups in the N0 structure, but other functional types can also be the ORR active sites through the ring-opening of the C–N bond depending on experimental conditions.

Acknowledgements

This work was supported by the WCU program (R31-2008-000-10055-0) and the National Research Foundation of Korea (NRF) grant funded by the Korean Government (NRF-2010-0028718). We thank Prof. William A. Goddard (Caltech) for helpful discussions.

References

1 W. Sheng, H. A. Gasteiger and Y. Shao-Horn, *J. Electrochem. Soc.*, 2010, **157**, B1529–B1536.
2 J. K. Nørskov, J. Rossmeisl, A. Logadottir, L. Lindqvist, J. R. Kitchin, T. Bligaard and H. Jónsson, *J. Phys. Chem. B*, 2004, **108**, 17886–17892.
3 A. S. Aricò, S. Srinivasan and V. Antonucci, *Fuel Cells*, 2001, **1**, 133–161.
4 H. Gasteiger, S. Kocha, B. Sompalli and F. Wagner, *Appl. Catal., B*, 2005, **56**, 9–35.
5 E. J. Biddinger, D. Deak and U. S. Ozkan, *Top. Catal.*, 2009, **52**, 1566–1574.
6 K. Gong, F. Du, Z. Xia, M. Durstock and L. Dai, *Science*, 2009, **323**, 760–764.
7 S. Kundu, T. C. Nagaiah, W. Xia, Y. Wang, S. V. Dommele, J. H. Bitter, M. Santa, G. Grundmeier, M. Bron, W. Schuhmann and M. Muhler, *J. Phys. Chem. C*, 2009, **113**, 14302–14310.
8 K. R. Lee, K. U. Lee, J. W. Lee, B. T. Ahn and S. I. Woo, *Electrochem. Commun.*, 2010, **12**, 1052–1055.
9 S. Maldonado and K. J. Stevenson, *J. Phys. Chem. B*, 2005, **109**, 4707–4716.
10 P. H. Matter, L. Zhang and U. Ozkan, *J. Catal.*, 2006, **239**, 83–96.
11 P. H. Matter, E. Wang, M. Arias, E. J. Biddinger and U. S. Ozkan, *J. Mol. Catal. A: Chem.*, 2007, **264**, 73–81.
12 L. Qu, Y. Liu, J. B. Baek and L. Dai, *ACS Nano*, 2010, **4**, 1321–1326.
13 C. V. Rao, C. R. Cabrera and Y. Ishikawa, *J. Phys. Chem. Lett.*, 2010, **1**, 2622–2627.
14 N. P. Subramanian, X. Li, V. Nallathambi, S. P. Kumaraguru, H. Colon-Mercado, G. Wu, J. W. Lee and B. N. Popov, *J. Power Sources*, 2009, **188**, 38–44.
15 R. O'Hayre, S. Cha, W. Colella and F. Prinz, *Fuel Cell Fundamentals*, John Wiley & Sons, New York, 2005.
16 H. Niwa, K. Horiba, Y. Harada, M. Oshima, T. Ikeda, K. Terakura, J. Ozaki and S. Miyata, *J. Power Sources*, 2009, **187**, 93–97.
17 K. A. Kurak and A. B. Anderson, *J. Phys. Chem. C*, 2009, **113**, 6730–6734.
18 Y. Okamoto, *Appl. Surf. Sci.*, 2009, **256**, 335–341.
19 T. Ikeda, M. Boero, S.-F. Huang, K. Terakura, M. Oshima and J. Ozaki, *J. Phys. Chem. C*, 2008, **112**, 14706–14709.
20 R. Car and M. Parrinello, *Phys. Rev. Lett.*, 1985, **55**, 2471–2474.
21 B. Shan and K. Cho, *Chem. Phys. Lett.*, 2010, **492**, 131–136.
22 T. Jacob and W. A. Goddard, *ChemPhysChem*, 2006, **7**, 992–1005.
23 E. J. Biddinger and U. S. Ozkan, *J. Phys. Chem. C*, 2010, **114**, 15306–15314.
24 G. Kresse and J. Furthmüller, *Comput. Mater. Sci.*, 1996, **6**, 15–50.
25 J. P. Perdew, K. Burke and M. Ernzerhof, *Phys. Rev. Lett.*, 1996, **77**, 3865–3868.
26 P. E. Blöchl, *Phys. Rev. B: Condens. Matter*, 1994, **50**, 17953.
27 H. J. Monkhorst and J. D. Pack, *Phys. Rev. B: Solid State*, 1976, **13**, 5188–5192.
28 D. Geng, S. Yang, Y. Zhang, J. Yang, J. Liu, R. Li, T. K. Sham, X. Sun, S. Ye and S. Knights, *Appl. Surf. Sci.*, 2011, **257**, 9193–9198.
29 D. Jiang, B. G. Sumpter and S. Dai, *J. Chem. Phys.*, 2007, **126**, 134701.
30 H. Jonsson, G. Mills and K. W. Jacobsen, *Classical and Quantum Dynamics in Condensed Phase Simulations*, 1998.
31 Z. Shi, J. Zhang, Z. Liu, H. Wang and D. Wilkinson, *Electrochim. Acta*, 2006, **51**, 1905–1916.
32 S. Chan, G. Chen, X. Gong and Z.-F. Liu, *Phys. Rev. Lett.*, 2003, **90**, 6–9.
33 R. J. Taylor and A. A. Humffray, *J. Electroanal. Chem.*, 1975, **64**, 85–94.
34 R. J. Taylor and A. A. Humffray, *J. Electroanal. Chem.*, 1975, **64**, 63–84.
35 H. Tominaga, W. Ikeda and M. Nagai, *Phys. Chem. Chem. Phys.*, 2011, **13**, 2659–2662.
36 J. Xu, W. Huang and R. L. McCreery, *J. Electroanal. Chem*, 1996, **410**, 235–242.
37 E. Yeager, *Electrochim. Acta*, 1984, **29**, 1527–1537.

